GEOPHYSICAL RESEARCH LETTERS, VOL. 17, NO. 10, PAGES 1653-1656, SEPTEMBER 1990

COMPARISON OF PLASMA WAVE MEASUREMENTS IN THE BOW SHOCKS AT EARTH, JUPITER, SATURN, URANUS AND NEPTUNE

S. L. Moses, F. V. Coroniti and C. F. Kennel

TRW Space and Technology Group

W. S. Kurth and D. A. Gurnett

Department of Physics and Astronomy, University of Iowa

Abstract. We present plasma wave measurements from the Voyager 2 crossing of Neptune's bow shock and compare them with measurements from the bow shocks of Earth, Jupiter, Saturn and Uranus. The wave amplitudes above $0.01f_p$, when normalized to the solar wind ion thermal energy density at each planet, are significantly higher at the outer planets than at Earth. Despite the differences in amplitude the shock spectra of all the planets can be fitted to curves of similar form in this frequency range. The total normalized electric field energy densities exhibit an exponential dependence on ion thermal Mach number. Magnetosheath wave energies are comparable at all of the planets when normalized to the downstream plasma pressure.

Introduction

Since the discovery of electrostatic waves in the Earth's bow shock by investigators on OGO-V (Fredricks et al., 1968), the generation of plasma waves in shocks and their role in microphysical shock processes have been the subject of much research and debate. Planetary bow shocks encountered by the Voyager spacecraft have provided examples of extremely strong shocks in solar wind parameter regimes rarely found at 1 AU. By comparing quantitatively the plasma wave spectra from representative crossings of the bow shocks at Earth, Jupiter, Saturn, Uranus and Neptune, we will show that in properly normalized units the wave amplitudes of electrostatic waves at the outer planets can be several orders of magnitude higher than at Earth, and thus are more likely to be significant participants in the shock processes than their terrestrial equivalents.

In the next section we discuss the Voyager bow shock data from the encounter with Neptune, and in the following section we compare wave amplitudes and spectral shapes from each of the planets. In the last two sections we analyze magnetosheath emissions and summarize our results.

Neptune Bow Shock Data

Figure 1 presents the data from the plasma wave detector (PWS) for the inbound bow shock crossing made during the Voyager 2 encounter with Neptune on August 24, 1989. Contained in the figure are electric field amplitudes in the bottom eight frequency channels of the 16-channel wave analyzer. Each spectrum requires 4 seconds to complete, and, although interference from spacecraft systems has been removed as thoroughly as possible, relatively large electric field levels are still evident in the 178- and 311-Hz channels, which are interpretted as residual interference from the spacecraft.

The leading edge of the shock foot is first detected at 1434 with the appearance of broadband emissions below f_p (600 Hz for the measured upstream density of 0.0045 cm^{-3}); 48-s average magnetometer (MAG) measurements indicate that the ramp is crossed beginning at 1438. The duration of the shock foot crossing at Neptune is significantly shorter than the foot transit time for the Voyager 2 inbound shock crossing at Uranus (approximately 15-min.), which suggests that this shock was moving rapidly towards the spacecraft. Gosling and Thomsen (1985) derived an expression for computing the shock velocity using the time taken to cross the shock foot and assuming that the ion beam that defines the shock foot is generated by specular reflection. For the upstream magnetic field strength of 0.12 nT (Ness et al., 1989), the solar wind speed of 403 km/s (Belcher et al., 1989), and assuming a nearly perpendicular shock, we obtain a shock speed of 132 km/s, so that the solar wind speed in the shock frame is 535 km/s.

In the average MAG data the shock ramp extends from 1438 to 1442 although higher resolution plasma and magnetic field measurements will prob-

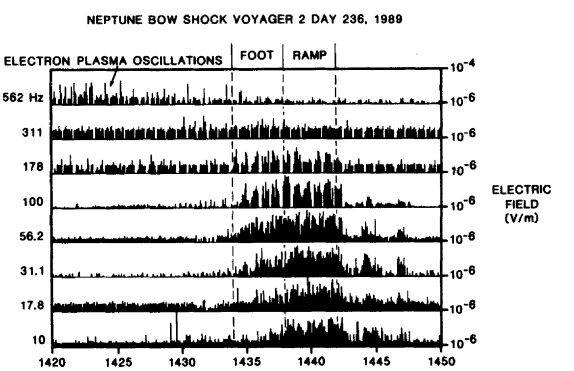

Fig. 1. PWS channel analyzer data for the Voyager 2 inbound crossing of Neptune's bow shock. Indicated on the plot are the location of the shock foot and ramp based on 48-s average MAG data.

Paper number 90GL00612;
0094-8276/90/90GL-00612$03.00

ably contract this time span. The entire foot and ramp region is filled with broadband emissions extending up to the plasma frequency. Beyond this region the wave levels decline rapidly, and, except for some isolated but prominent emissions in the overshoot at 1444 and 1447, downstream is essentially quiet. The apparent absence of magnetosheath emissions is characteristic of the shocks at the outer planets and quite unlike the terrestrial magnetosheath, which is usually filled with broadband electrostatic waves.

Comparison of Shock Spectra

In order to make comparisons between the bow shocks observed at the Earth and outer planets, we have chosen previously studied inbound bow shock crossings from each planet. The terrestrial bow shock is the ISEE-1, November 7, 1977 crossing (Scudder et al., 1986), the Jovian bow shock is the Voyager 1, March 1, 1979 crossing (Moses et al., 1985), the Saturnian bow shock is the Voyager 1, November 11, 1980 crossing (Moses et al., 1988) and the Uranian bow shock is the Voyager 2, January 24, 1986 crossing (Bagenal et al., 1987). All of these shocks are supercritical, quasiperpendicular events and exhibit the shock foot and overshoot associated with ion reflection. Table 1 provides upstream parameters that will be used in our analysis. Ion parameters have been chosen, since the Voyager plasma science experiment (PLS) is unable to measure electrons in the solar wind upstream of shocks at Uranus and Neptune due to their low energy flux. In any case, solar wind T_e and T_i usually differ by significantly less than an order of magnitude. Solar wind speeds have been augmented with estimations of the shock speed for each planet except Uranus, where the shock speed was determined to be negligible.

Table 1. Upstream Plasma Parameters

Parameter	Earth	Jupiter	Saturn	Uranus	Neptune
n_{sw} (cm^{-3})	9.87	0.44	0.11	0.05	0.0045
T_i (1000 K)	69	7.9	15	49	6.3
B_{sw} (nT)	5.49	0.8	0.4	0.19	0.12
V_{sw} (km/s)	292*	610*	617*	430	535*

*Indicates that V_{sw} has been augmented by an estimation of the shock speed.

In the top panel of Figure 2 we present the plasma wave spectrum for each of these shocks for frequencies up to the solar wind f_p. The spectrum is an average over the strongest signals (corresponding roughly to the shock foot, ramp and overshoot regions). The vertical axis plots spectral density (V^2/m^2-Hz) versus frequency with circles representing Earth, triangles representing Jupiter, diamonds representing Saturn, inverted triangles representing Uranus and squares representing Neptune. Each shock exhibits a broad peak, more nearly a plateau for the terrestrial example, that falls off sharply at high frequency. The peak frequency diminishes with radial distance and decreasing solar wind density, which is consistent with the high frequency

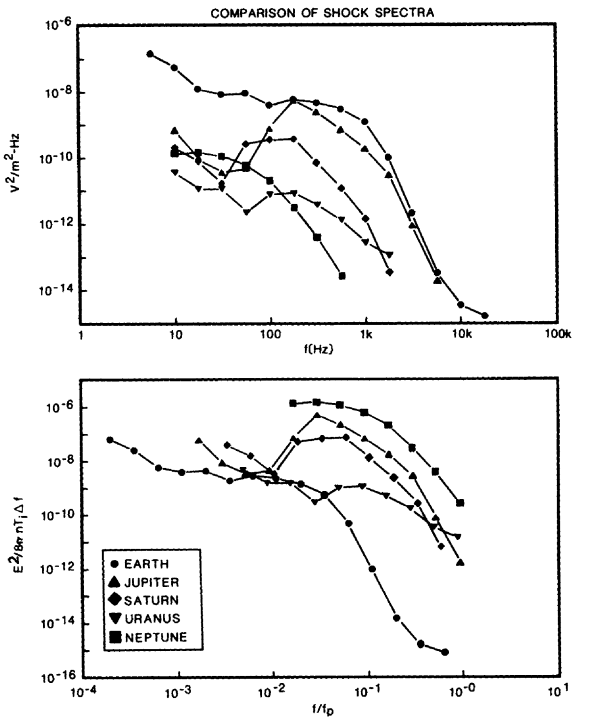

Fig. 2. Comparison of shock spectra for Earth (circle), Jupiter (triangle), Saturn (diamond), Uranus (inverted triangle) and Neptune (square). The top panel shows the spectral density as a function of frequency for frequencies below the solar wind plasma frequency. In the bottom panel the spectral densities are converted to wave energy densities and normalized to the solar wind ion thermal energy density. The frequencies are normalized to the solar wind plasma frequency.

waves being primarily electrostatic and scaling in frequency as f_p. The wave amplitudes generally diminish with increasing radial distance from the sun; however, the wave amplitudes at Uranus are the smallest, and Moses et al. (1989) has suggested that this due to unusual solar wind conditions, $T_e < T_i$, which renders it difficult for electrostatic waves to grow.

We improve this comparison in the bottom panel by normalizing wave frequencies to the solar wind f_p and wave energy densities/frequency to the solar wind ion thermal energy density. For frequencies above 0.01 f_p the normalized amplitudes of the outer planet bow shocks are much stronger relative to the Earth. Since waves in this frequency range must certainly resonate with electrons, electrostatic wave-particle interactions at the outer planets may be significantly more effective in producing shock dissipation than their analogs at Earth.

Despite the differences in normalized wave amplitudes, all of the shocks exhibit a similar high frequency falloff. We have examined the shape of the spectra by fitting the falloff to curves of the form:

$$S = S_o \exp\{ -[(f - f_o)/f_1]^{\alpha} \}$$

S_o and f_o are the spectral density and frequency for the peak in the spectrum, and linear regression is used to determine f_1 (which scales the bandwidth of the peak) and α (which determines the rate of falloff). Table 2 gives the values of f_o and f_1 (normalized to f_p) and α used. Earth required special treatment, since the spectrum appears more as a plateau than a peak. At the outer planets f_o/f_p ranges between 0.03 and 0.09, which is slightly above the proton plasma frequency of 0.023 f_p. Only two frequency channels at Earth fall into this range, 1 kHz and 1.78 kHz, and the fit was performed assuming f_o = 1 kHz. The correlation coefficient from each regression was > 0.99. One finds that the curve parameters for each spectrum are very similar, which makes it likely that the physics determining the shape of the shock spectrum at high frequencies is analogous throughout the heliosphere.

Table 2. Comparison of Curve Fitting Results

Parameter	Earth	Jupiter	Saturn	Uranus	Neptune
f_o/f_p	0.0353	0.0298	0.0597	0.0886	0.0295
f_1/f_p	0.0059	0.027	0.021	0.086	0.076
α	0.738	0.736	0.682	0.795	0.955

We compare the total normalized wave energy densities above 0.01 f_p by multiplying the peak normalized spectral densities by f_1. In Figure 3 we plot this quantity as a function of V_{sw}/a_i, where a_i is the ion thermal speed. These points can be fitted with an exponential curve of the form $\exp[\kappa V_{sw}/a_i]$, where κ is determined to be 0.15. This result was unexpected, but suggests a general scaling law for plasma wave amplitudes in shocks. The interpretation of this apparent scaling probably involves a detailed analysis of wave convective growth and saturation, and will be pursued in future work.

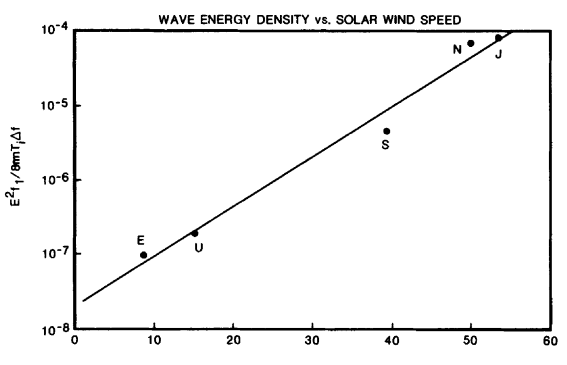

Fig. 3. Total peak normalized wave energy density as a function of ion thermal Mach number. The peak normalized energy density was obtained by multiplying the peak normalized spectral density by the computed bandwidth of the high frequency falloff. The points are fitted to an exponential curve.

Comparison of Magneotsheath Spectra

Outer planet shocks exhibit an apparent absence of magnetosheath emissions (Scarf et al., 1979). In the top panel of Figure 4 we present spectra immediately downstream of the shock overshoot. The wave spectral densities at Earth can be as much as five orders of magnitude greater than those observed at the outer planets. Most of the outer planet spectra are very near the background level of the Voyager instrument, particularly at high frequencies (the threshold level of the PWS is indicated by a dashed line). Only the Uranian bow shock exhibits significant emissions in this region, and this shock was unusual for the long duration and ragged appearance of the shock crossing in the plasma wave data (Moses et al., 1989).

The Rankine-Hugoniot relations indicate that in a strong shock the downstream plasma pressure is proportional to $0.5nm_iV_{sw}^2$, and in heliospheric shocks the main contribution to the downstream pressure is the ion thermal energy density. The spectral densities are normalized to $0.5nm_iV_{sw}^2$ in the bottom panel. The frequencies have also been normalized to the downstream f_p. Upon normalization the wave levels at the outer planets now become more nearly comparable to the terres-

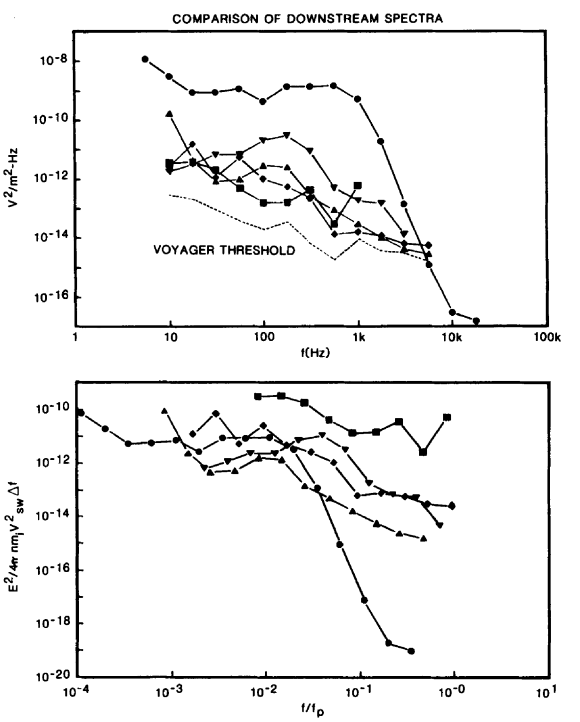

Fig. 4. Comparison of downstream spectra. One-minute average downstream spectra are shown. In the top panel spectral densities are plotted against frequency. A dashed line indicates the Voyager PWS threshold. In the bottom panel the spectral densities are normalized to upstream ram pressure, which is proportional to the downstream plasma pressure in strong shocks, and the frequencies are normalized to the downstream plasma frequency.

trial magnetosheath below approximately $0.03f_p$, and at these frequencies the outer planets no longer form a discreet subset of spectra. At higher frequencies the outer planets have much higher wave levels, but at these frequencies the outer planet wave levels are indistinguishable from the background noise in the detector and may not represent the true magnetosheath amplitudes. If, as Figure 4 suggests, the strength of the magnetosheath waves may not be greatly different at each of the planets when normalized to the downstream plasma pressure, then the downstream state of the plasma is essentially the same for all of the planets, and we need not attempt to create theories that differentiate between the shocks at Earth and the outer planets.

Summary

By comparing the shock and magnetosheath spectra of bow shocks at Earth, Jupiter, Saturn, Uranus and Neptune we have been able to draw the following conclusions.

1. While the spectral densities of plasma waves tend to decrease with radial distance from the sun, when normalized to upstream nT_i the wave levels at the outer planets are significantly higher above $0.01f_p$.

2. The high frequency falloff of the plasma wave spectra of all of the planets have similar shapes. This suggests that the physical processes governing the spectral shape are the same for shocks throughout the heliosphere.

3. The total normalized wave energy density for high frequency waves increases exponentially with increasing V_{sw}/a_i.

4. The wave amplitudes in the magnetosheaths of the outer planets do not differ significantly from the amplitudes at Earth when normalized to the downstream plasma pressure below $0.03\ f_p$. This suggests that the apparent absence of downstream waves at the outer planets is more a function of the instrument sensitivity than differences in the wave generation physics.

Acknowledgments. The work at TRW was supported by JPL Contract 957805, and at the University of Iowa by JPL Contract 957723.

References

Bagenal, F., et al., The Uranian bow shock: Voyager 2 observations of a high Mach number shock, J. Geophys. Res., 92, 8603-8612, 1987.

Belcher, J. W., et al., Plasma observations near Neptune: Initial results from Voyager 2, Science, 246, 1478-1483, 1989.

Fredricks, R. W., et al., Detection of electric field turbulence in the Earth's bow shock, Phys. Rev. Lett., 21, 1761, 1968.

Gosling, J. T., and M. F. Thomsen, Specularly reflected ions, shock foot thicknesses, and shock velocity determinations in space, J. Geophys. Res., 90, 9893-9896, 1985.

Moses, S. L., et al., High time resolution plasma wave and magnetic field observations of the Jovian bow shock, Geophys. Res. Lett., 12, 183-186, 1985.

Moses, S. L., et al., Wave-particle interactions in the foot of the Saturnian bow shock, J. Geophys. Res., 93, 1785-1793, 1988.

Moses, S. L., et al., Electrostatic waves in the bow shock at Uranus, J. Geophys. Res., 94, 13,367-13,376, 1989.

Ness, N. F., et al., Magnetic fields at Neptune, Science, 246, 1473-1478, 1989.

Scarf, F. L., et al., Jupiter plasma wave observations: An initial Voyager 1 overview, Science, 204, 991-995, 1979.

Scudder, J. D., et al., The resolved layer of a collisionless, high β, supercritical, quasi-perpendicular shock wave, 1, Rankine-Hugoniot geometry, currents, and stationarity, J. Geophys. Res., 91, 11,019-11,052, 1986.

F. V. Coroniti, C. F. Kennel and S. L. Moses TRW S&TG R1/1170, One Space Park, Redondo Beach CA 90278

D. A. Gurnett and W. S. Kurth, Dept. of Physics and Astronomy, University of Iowa, Iowa City IA 52242

(Received February 20, 1990;
Accepted March 5, 1990)